Precise Geometric Registration of Aerial Imagery and LIDAR Data

Kyoungah Choi, Juseok Hong, and Impyeong Lee

In this paper, we develop a registration method to eliminate the geometric inconsistency between the stereo-images and light detection and ranging (LIDAR) data obtained by an airborne multisensor system. This method consists of three steps: registration primitive extraction, correspondence establishment, and exterior orientation parameter (EOP) adjustment. As the primitives, we employ object points and linked edges from the stereo-images and planar patches and intersection edges from the LIDAR data. After extracting these primitives, we establish the correspondence between them, being classified into vertical and horizontal groups. These corresponding pairs are simultaneously incorporated as stochastic constraints into aerial triangulation based on the bundle block adjustment. Finally, the EOPs of the images are adjusted to minimize the inconsistency. The results from the application of our method to real data demonstrate that the inconsistency between both data sets is significantly reduced from the range of 0.5 m to 2 m to less than 0.05 m. Hence, the results show that the proposed method is useful for the data fusion of aerial images and LIDAR data.

Keywords: Registration, correspondence, bundle adjustment, data fusion, image, LIDAR.

Manuscript received Dec. 31, 2010; revised Mar. 15, 2011; accepted May 3, 2011.

This research was supported by a grant (07KLSGC03) from Cutting-edge Urban Development–Korean Land Spatialization Research Project funded by Ministry of Land, Transport and Maritime Affairs.

Kyoungah Choi (phone: +82 2 2210 5299, email: shale@uos.ac.kr) and Impyeong Lee (corresponding author, email: iplee@uos.ac.kr) are with the Department of Geoinformatics, University of Seoul, Seoul, Rep. of Korea.

Juseok Hong (email: jshong81@gmail.com) is with the Technical Research Center, GSM Solutions, Seoul, Rep. of Korea.

doi:10.4218/etrij.11.1610.0046

I. Introduction

The increasing demand for up-to-date and precise 3D models, particularly for urban areas, encourages us to do research on establishing and providing spatial information such as digital surface models (DSMs), orthoimages, and city models. This spatial information can be efficiently generated using the data acquired by multisensor systems. There exist several different types of available multisensor systems which include airborne systems based on manned/unmanned aerial vehicles or ground systems based on wheeled vehicles [1]. Those multisensor systems are usually equipped with global positioning system (GPS)/inertial navigation system (INS), a camera, and a laser scanner [2]. Especially, an airborne multisensor system, which is carrying GPS/INS, a camera, and a laser scanner, facilitates producing sophisticated 3D models autonomously and cost-effectively [3].

Numerous studies attempt to reconstruct the object space by employing LIDAR data and aerial imagery simultaneously due to their complementary characteristics [4]. The important advantages of LIDAR systems are direct acquisition of 3D coordinates from ground objects and better vertical accuracy than horizontal accuracy. However, they may have difficulties obtaining the information along break lines. On the other hand, camera systems enable us to derive dense spatial information along the break lines and their horizontal accuracy is superior to the vertical accuracy. Nonetheless, it is hard to construct dense 3D coordinates from only aerial imagery because of the absence of robust and reliable matching procedures [5]. Thus, the majority of existing research related to the generation of 3D city models takes advantage of such complementary characteristics [6]-[9]. In addition, changes in urban areas are detected and ancient ruins are reconstructed by exploiting

synergic effectiveness of both kinds of data [10], [11].

The synergy of LIDAR data and images can be fully utilized only after the elimination of the geometric inconsistency between both kinds of data, called geometric registration [12]. The inconsistency originates from the systematic errors of each individual sensor. For example, the errors are inherent in interior orientation parameters (IOPs) of a camera, exterior orientation parameters (EOPs) of images, internal parameters of a laser scanner, and so on. To reduce or eliminate the inconsistency, we should address the following issues.

- Extraction of registration primitives
- Correspondence setup between the primitives
- Transformation of the matched entities

The primitives to be used to establish the correspondence between both datasets are the points, linear features, and areal features. The significant issue in the determination of the primitives is the fact that the primitives can be extracted and identified automatically and accurately. The correspondence between conjugate primitives is found by the similarity measure, which describes the correspondence of conjugate entities mathematically. It is also important to find the correspondence automatically because this task can be laborious for a situation where there is an enormous amount of data, including images and LIDAR data. We compute the 3D location of the matched entity and transform the entity to a reference frame at the end of the registration procedure.

A number of registration methods have been developed in the past few years. Some methods use point primitives. The iterative closest point method solves the registration problem by matching dense photogrammetric point cloud to LIDAR point cloud [13], [14]. In this case, it is difficult to find the correspondence between each primitive set due to the irregular nature of the LIDAR points and require extensive overlapping images. To alleviate the difficulty in finding the correspondence, some methods utilize special targets which can be effortlessly detected in range images [15], [16]. However, there is still the restriction on the automation of the procedure and the needs of special targets.

Planar patch-to-patch registration methods which use areal features as the primitive have been accomplished [17], [18]. The analysis of the elevation at corresponding grid posts is executed in the procedure. Therefore, the interpolation into a grid can produce some errors. The registration method using centroid of the roof surfaces of buildings extracted from LIDAR data and images is proposed [19]. The correspondence established in this method lacks reliability. In addition, planar patch-to-point registration methods are found [20], [21]. When planar patches extracted from images are used, the extraction process is not reliably automated. Also, when planar patches automatically generated from LIDAR data are used, it tends to minimize the differences mostly along the vertical direction rather than horizontal direction. This limitation mainly occurs because most planar patches extracted from LIDAR data are nearly horizontal.

To mitigate the various problems mentioned above, many researchers focus on the use of linear primitives. Three connected segments (3CS), consisting of connected line segments, are detected from both kinds of data and then matched [22]. The registration is achieved by comparing 2D linear primitives from images with 3D linear primitives from LIDAR data [23]-[26]. Those approaches usually apply an edge detector, such as the Canny operator, to images to obtain the 2D linear primitives. 3D linear primitives from LIDAR data are created by the segmentation and intersection of patches. They can minimize the differences between images and LIDAR data along both horizontal direction and vertical direction through adjusting EOPs of images or estimating transformation parameters. Approaches based on the linear primitives are not completely satisfied in terms of accuracy. Horizontal accuracy is remarkably improved by adopting linear primitives. Nevertheless, the inevitable error along a vertical direction can remain since those linear primitives are mainly located at the intersection of two facets of gable-frame roofs. The seaming structure on the intersection results in the vertical difference between the primitives from images and LIDAR data.

This paper introduces an alternative methodology for geometric registration of aerial images and LIDAR data. Our methodology employs two kinds of the combination of primitives to be compared for more precise registration. One is the linear-to-linear comparison for the minimization of the horizontal difference. The other is the areal-to-point comparison as vertical constraints. All of the primitives can be extracted from each dataset automatically and incorporated into the bundle block adjustment with stochastic constraints simultaneously. The following section explains the general methodology and mathematical model of our proposed approach. Section III covers the experimental results using real data. Finally, section IV highlights the research conclusions and recommendations for future work.

II. Registration Methodology

The geometric inconsistency between multisensory data usually originates from the systematic errors still remaining in each individual sensory data even after their precise calibration process. To combine such inconsistent multisensory data for any data fusion process, we should first eliminate such inconsistency through a precise registration of these data.

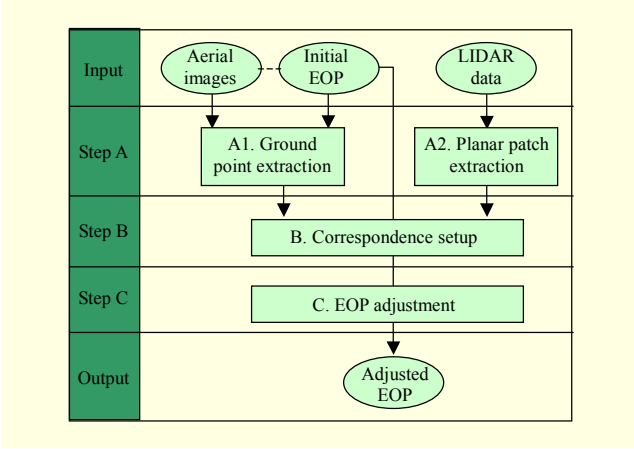

Fig. 1. Outline of proposed registration process.

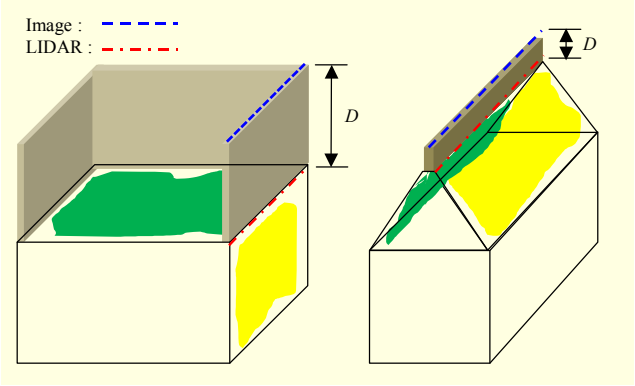

Fig. 2. Vertical inconsistency between linear primitives from imagery and LIDAR data.

The proposed registration process of aerial images and LIDAR data consists of three main steps; namely, primitive extraction, correspondence setup, and EOP adjustment [27], as shown in Fig. 1. These steps will be explained in the following subsections.

1. Extraction of Registration Primitives

The registration primitives are the geometric features extracted from both data sets and used for registration afterward. In general, a registration process attempts to minimize the discrepancies systematically existing between conjugate primitives from both data sets. Such primitives should be easily identifiable and possibly automatically extractable. They should also represent some portions of the object space exactly and be evenly located on the target area if possible. In imagery and LIDAR data, different characteristics of both data sets may require more deliberate selection of the registration primitives. For example, an image consists of a set of gray values regularly distributed on a 2D image plane, while LIDAR data comprises a set of points irregularly distributed on the 3D object space.

In this research, as the registration primitives, linear and areal features are used. The different combinations of such primitives are used to minimize the inconsistency along vertical and horizontal directions, respectively. This can overcome the limitation of the existing methods employing linear or areal features as the primitives. For example, the point-to-patch methods efficiently remove the difference along the vertical direction but may not control the differences along the horizontal direction. Also, in the line-to-line methods, the vertical correspondences between the conjugate line pairs may often be incorrect though their horizontal correspondences are accurate. Such examples are illustrated in Fig. 2. Linear features from each dataset can be extracted at the break lines, such as the boundaries of buildings or the intersection of two facets of gable-frame roofs. Usually, the line-to-line methods attempt to also eliminate the vertical difference as well as horizontal difference, even though the vertical differences are real, not originating from the systematic errors. Such differences can occur due to the balustrades on the top of buildings or the seaming structures on the center of gable-frame roofs, as shown in Fig. 2. Thus, we reduce only the horizontal differences using linear primitives and the vertical difference by the point-to-patch approach.

The primitives from stereo-images are the object points derived from the tie points selected from the stereo-images and the 3D edges linking the object points. From the tie points, the object points can be computed using the collinearity equations with the initial EOPs provided from GPS/INS. The tie points are selected on two different types of areas. The first type includes relatively flat, smooth, and large areas, such as roads regions and parking lots, mainly contributing to controlling the vertical discrepancies. The tie points of the other type are mainly located on the break lines, such as the boundaries of buildings and the intersection of two facets of gable-frame roofs, to control horizontal coordinate. The object points from the tie points are linked for 3D intersected edges to be utilized as the registration primitives.

The primitives from the LIDAR data are the planar surface patches segmented from the raw LIDAR points and the intersection edges derived from the adjacent patches. The segmentation can be performed by recursively grouping the points near to each other with similar plane parameters based on the theory of perceptual organization [28]. Each patch is then described with a set of plane parameters, the fitting errors, and its boundary. The primitives from LIDAR data are classified into two groups, similarly to the primitives from stereo-images. The first group is the planar patches, located on flat areas, such as roads and parking lots. These areal primitives are utilized to control vertical discrepancies along the vertical

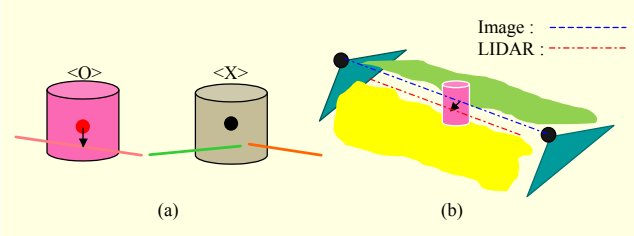

Fig. 3. Illustration of finding correspondence between (a) patches and points and (b) linked and intersected edges.

direction. The second group consists of 3D edges, which are intersected with two patches of gable-frame roofs. These linear primitives are employed to compare the differences of the horizontal coordinates.

2. Correspondence Setup

After extracting the registration primitives from the aerial images and LIDAR data, their correspondences are then established, mainly using the distance among the registration primitives. For the comparison of the vertical difference, we have to establish the correspondence between the 3D object points derived from aerial images and the planar patches generated from the LIDAR data. To assign the patch to point correspondence, we first select almost horizontal patches of large areas and small fitting errors. The road regions are major candidates for those patches which almost retain no variation of height and low roughness. Then, the correspondence is assigned if all the image-derived object points are within the boundary of each patch. Considering the uncertainty, which is inherent in the estimated object point coordinates from initial EOPs given by GPS/INS, the confidence interval of the assignment is determined, as illustrated in Fig. 3(a). If another patch exists in the confidence interval or the vertical difference between the corresponding object point and the patch is significant, the assignment of the correspondence is invalidated. However, to compare horizontal coordinates, it is essential to individually find 3D corresponding lines from each dataset. To assign the correspondence between the image-derived 3D edges and LIDAR-derived intersection edges, we check the distance between the edges and assign the correspondence to any pair of the edges close to each other. If the vertical distance between the linked edge from an image and the intersected edge from LIDAR data is slight and the horizontal distance is in a confidence range, the correspondence between two edges is established, as illustrated in Fig. 3(b). The confidence range is determined by the uncertainty derived from the fitting error of the patch and the estimation error of the end points of the edge from images based on the error propagation principle.

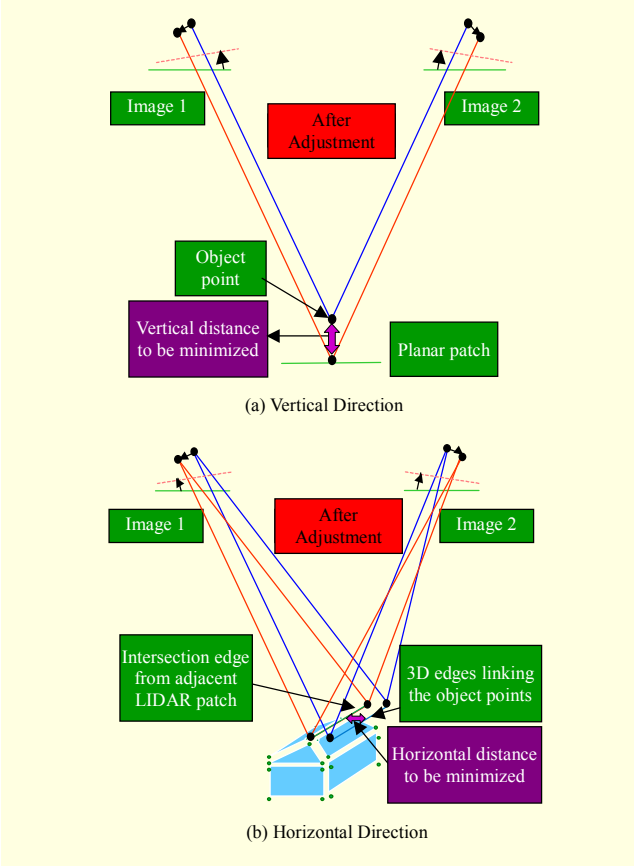

Fig. 4. Proposed adjustment model.

3. EOPs Adjustment

Ideally, the object points should be located exactly on their corresponding patches. In reality, this is not the case because of the registration errors between the data sets. Also, the corresponding pairs of the edges should be coincident at least for the horizontal location. The horizontal patches are used as the vertical control while the intersected edges are used as the horizontal control to adjust the EOPs. With this control information, the tie points and GPS/INS data, we perform the bundle block adjustment to adjust the EOPs and the coordinates of the object points. This adjustment model is illustrated in Fig. 4.

The mathematical model for the adjustment of EOPs is based on the collinearity equations, which are functions of the interior orientation parameters (I), the exterior orientation parameters (E), and the ground points (P):

$$p = f(I, E, P), \tag{1}$$

where p is the vector of the conjugate points.

Using the conjugate points, IOPs, and initial EOPs provided by GPS/INS, the observation equations with the stochastic constraints are established as

$$\begin{bmatrix} y \\ z \end{bmatrix} = \begin{bmatrix} A_e & A_p \\ K_e & 0 \end{bmatrix} \begin{bmatrix} \xi_e \\ \xi_p \end{bmatrix} + \begin{bmatrix} e_y \\ e_z \end{bmatrix}, \quad \begin{bmatrix} e_y \\ e_z \end{bmatrix} \sim \left(\begin{bmatrix} 0 \\ 0 \end{bmatrix}, \begin{bmatrix} D_y & 0 \\ 0 & D_z \end{bmatrix} \right) \tag{2}$$

where y is the observations composed of conjugate points; z is the constraint imposed on EOPs, provided from GPS/INS; A_e and A_p are the design matrices derived from the partial differentiation of the collinearity equations with respect to the parameters ξ_e and ξ_p ; K_e is the design matrix related to the constraints; e_y and e_z are the error vectors associated with the corresponding observation vectors; and finally, D_y and D_z are the dispersion matrices of the error vectors.

By performing the aerial triangulation without GCPs based on the observation equations, the EOPs as well as the coordinates of the object points are estimated. The estimated object points and 3D edges linking them are the photogrammetric primitives for the registration procedure.

To minimize the inconsistency between photogrammetric primitives and LIDAR primitives, this method employs ground control patches and lines instead of ground control points. The control patches are the planar patches generated from LIDAR data and the control lines are the lines of the intersection of the patches. The observation equations including the control features as stochastic constraints for the aerial triangulation are

$$\begin{bmatrix} y \\ z \\ v \\ h \end{bmatrix} = \begin{bmatrix} A_e & A_p \\ K_e & 0 \\ 0 & K_v \\ 0 & K_h \end{bmatrix} \begin{bmatrix} \xi_e \\ \xi_p \end{bmatrix} + \begin{bmatrix} e_y \\ e_z \\ e_v \\ e_h \end{bmatrix}, \quad \begin{bmatrix} e_y \\ e_z \\ e_v \\ e_h \end{bmatrix} \sim \left(\begin{bmatrix} 0 \\ 0 \\ 0 \\ 0 \end{bmatrix}, \begin{bmatrix} D_y & 0 & 0 & 0 \\ 0 & D_z & 0 & 0 \\ 0 & 0 & D_v & 0 \\ 0 & 0 & 0 & D_h \end{bmatrix} \right), \tag{3}$$

where v and h are the observation vectors for the vertical and horizontal constraints, respectively; K_v and K_h are the design matrices denoting the relationship v/h and ξ_p ; e_v and e_h are the error vectors implying the uncertainty of the constraints; the expectation of the error vectors is zero; and their dispersions are D_v and D_h, respectively.

The vertical constraint is expressed mathematically as

$$Z = aX + bY + c\,. \tag{4}$$

The vertical constraint is that an object point (X, Y, Z), derived from a pair of conjugate points, has to locate on the corresponding planar patch with plane coefficients (a, b, c). To substitute (4) into (3), (4) can be rewritten as

$$-c = \begin{bmatrix} a & b & -1 \end{bmatrix} \begin{bmatrix} X \\ Y \\ Z \end{bmatrix} + e_{vi}, e_{vi} \sim (0, \sigma_i^2). \tag{5}$$

In (5), $-c$, $\begin{bmatrix} a & b & -1 \end{bmatrix}$, and $\begin{bmatrix} X & Y & Z \end{bmatrix}^T$ indicate v, K_v, and ξ_p , respectively. The error vector is denoted by e_{vi}, which means the uncertainty of the vertical constraint. Its dispersion coincides with the roughness of the patch, represented as σ_i^2 .

More than two object points on the 3D edge derived from images have to coincide with the corresponding intersection edge from adjacent patches. This horizontal constraint is expressed mathematically as

$$(a_1 - a_2)X + (b_1 - b_2)Y + (c_1 - c_2) = 0\,. \tag{6}$$

The coefficients of the adjacent two patches are (a_1, b_1, c_1) and (a_2, b_2, c_2). The horizontal coordinates of an object point on the 3D photogrammetric edge are (X, Y). To substitute (6) into (3), (6) can be also rewritten as

$$(c_2 - c_1) = \begin{bmatrix} (a_1 - a_2) & (b_1 - b_2) & 0 \end{bmatrix} \begin{bmatrix} X \\ Y \\ Z \end{bmatrix} + e_{hi}, \quad e_{hi} \sim (0, \sigma_j^2 + \sigma_k^2) \tag{7}$$

From (7), $(c_2–c_1)$, $[(a_1–a_2), (b_1–b_2), 0]$, and $\begin{bmatrix} X & Y & Z \end{bmatrix}^T$ are represented by h, K_h ,and ξ_p , respectively. The error vector is e_{hi}, which denotes the uncertainty of the horizontal constraint. Its dispersion coincides with the sum of roughness (σ_j^2 , σ_k^2) of the adjacent two patches, which produce the intersection edge corresponding to the 3D photogrammetric edge.

Finally, we determine the exterior orientation parameters of all the images by applying the least squares principle to the observation equations.

III. Experimental Results

1. Experimental Data and Preprocessing

The test area is a small portion of Jeju Island, Korea, which includes buildings, roads, and mountains. From this area, we acquired the test data by an airborne multisensor system equipped with a medium format metric digital camera, a laser scanner, and a GPS/INS. All the sensors are precisely synchronized with the GPS time. The GPS/INS provides the initial approximations to the EOP of each image at its time of exposure. The test data includes a pair of stereo-images, LIDAR data, and the GPS/INS data. Figure 5 shows the ground coverage of these data.

As the digital camera is a metric camera, the focal length, the

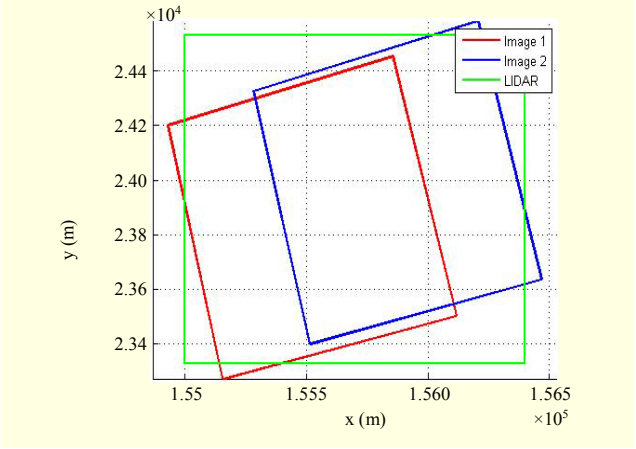

Fig. 5. Ground coverage of test imagery and LIDAR data.

Table 1. Key parameters of image acquisition.

Item	Value
Dimensions (pixels)	4,092 × 4,077
Pixel size (μm)	9.0
Focal length (mm)	55.145
Nominal height (m)	1,438
Nominal GSD (cm)	23
Nominal base length (m)	379
Nominal base/height ratio	0.264

Table 2. Key properties of LIDAR data.

Item	Value
Number of points (pts)	4,990,602
Point density (pts/m^2)	2.4
Nominal point interval (cm)	64
Average elevation (m)	175.1

location of the principle point, and the lens distortion parameters are provided from a camera calibration report. The key parameters of the image acquisition are shown in Table 1. The key properties of the LIDAR data are shown in Table 2. With the LIDAR points, we generated a DSM with the grid interval of 1 m.

2. Registration of Images and LIDAR Data

To check the geometric discrepancy between the aerial images and LIDAR data, we first carefully selected 12 regions well distributed over the overlapping area of both sets of data, as denoted by A to L in Fig. 6. In each area, we manually

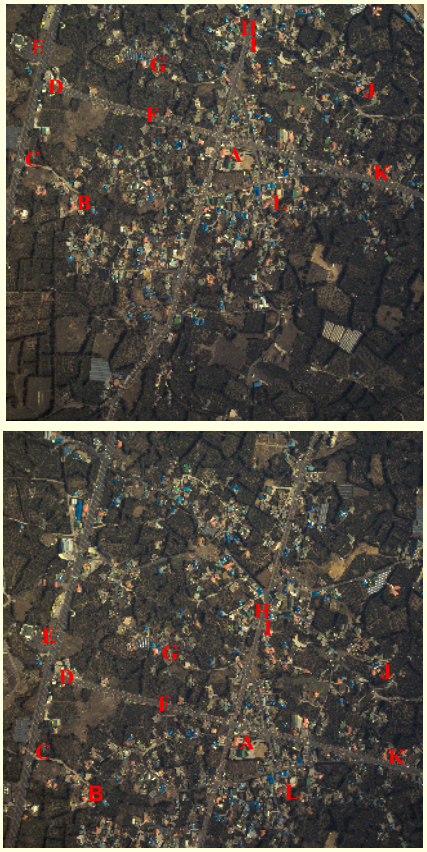

Fig. 6. Regions selected over overlapping area of both images and LIDAR data visualized on images 1 and 2.

Table 3. Types and numbers of tie points.

Region	Type	No.	Region	Type	No.
A	Building	14	G	Building	12
B	Building	16	H	Building	20
C	Road	11	I	Road	10
D	Road	13	J	Building	12
E	Building & road	18	K	Building	12
F	Road	5	L	Building & road	16
Sum					159

selected a number of pairs of tie points from both images by mainly digitizing easily distinguishable points on building roofs and roads. The types and number of the tie points in each area are listed in Table 3. In total, 159 pairs of tie point are selected from the 12 regions. Figure 7 shows the tie point selected on building roofs. When selecting the tie points on building roofs, we digitized the entire corner points of each roof patch so that we could reconstruct the full geometry of the building roof. While the primitives from the images are

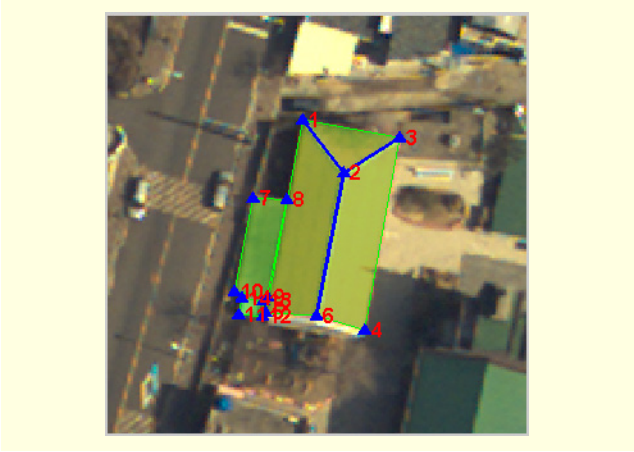

Fig. 7. Tie points selected on building roofs in region A.

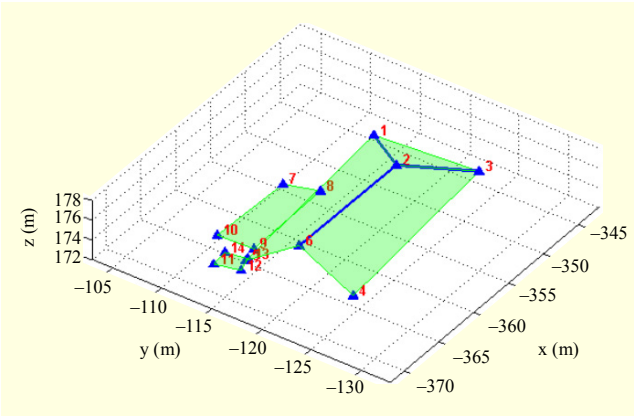

Fig. 8. Object points computed from tie points in region A.

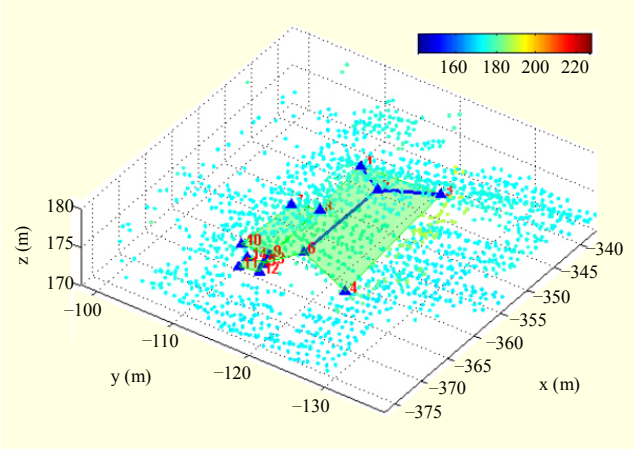

Fig. 9. LIDAR points and image derived object points in region A.

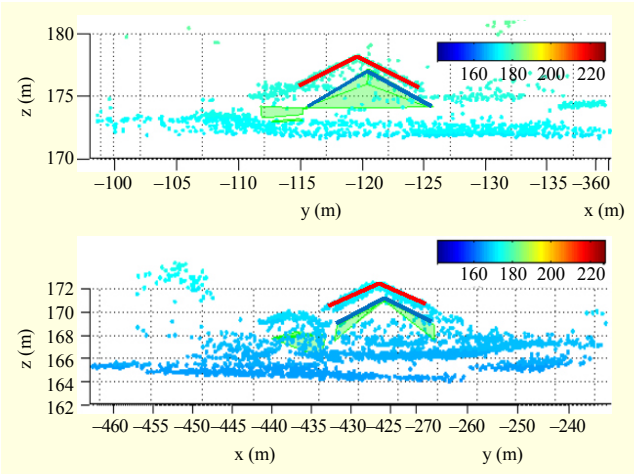

Fig. 10. Discrepancies between LIDAR points and image derived object points in regions A and L.

extracted manually, those from LIDAR data are automatically generated by the segmentation and intersection procedures [28].

By performing the bundle block adjustment with the constraints on the EOPs using the GPS/INS data, we estimated the EOPs of every image and the object points corresponding to every pair of tie points. By analyzing the variance-covariance matrix of the estimated parameters, we found that the precision of the vertical coordinates of the object points was much worse than that of the horizontal coordinates. This is because the original usage of the aerial images is just the texture mapping on the LIDAR derived DSM; hence, the base-height ratio is insufficient for the accurate geometric reconstruction. Figure 8 shows the object points in region A. The thick blue lines indicate intersected edges and the thin green lines do boundary edges. Based on the visual inspection on the roof geometry reconstructed with the object points, we also confirm the poor vertical accuracy. For example, the central intersection edge of the gable roof in Fig. 8 should be a horizontal line, but the vertical difference of the object point 2 and 6 is about 1.3 m. Conversely, in the 2D plot, the building boundary edges look quite parallel or orthogonal, indicating relatively good horizontal accuracy of the object points.

Around the image-derived object points in each region, we extract the LIDAR points, as shown as in Fig. 9. The colored points indicate the LIDAR points, in which the color represents the elevation of each point.

To show the geometric discrepancy between the LIDAR points and the image-derived object points, we visualize the data with a different view in Fig. 10. By comparing the roof lines (the solid red and blue lines) extracted from both sets of data, we can recognize a significant difference in both horizontal and vertical coordinates. Such discrepancies were similarly observed in other regions. These systematic discrepancies originate mainly from inaccurate system calibration parameters, especially bore-sight angles. Although both sets of bore-sight angles for photogrammetric and LIDAR systems are not accurate, the precise registration can be achieved by adjusting either EOPs of images or EOPs of LIDAR data to the other. In this study, we decided to adjust the

Table 4. Threshold values for correspondence setup.

Threshold		Value
Areal-to-patch correspondence	Vertical distance (m)	1
	Horizontal distance (m)	2
Linear-to-linear correspondence	Vertical distance (m)	2
	Horizontal distance (m)	1

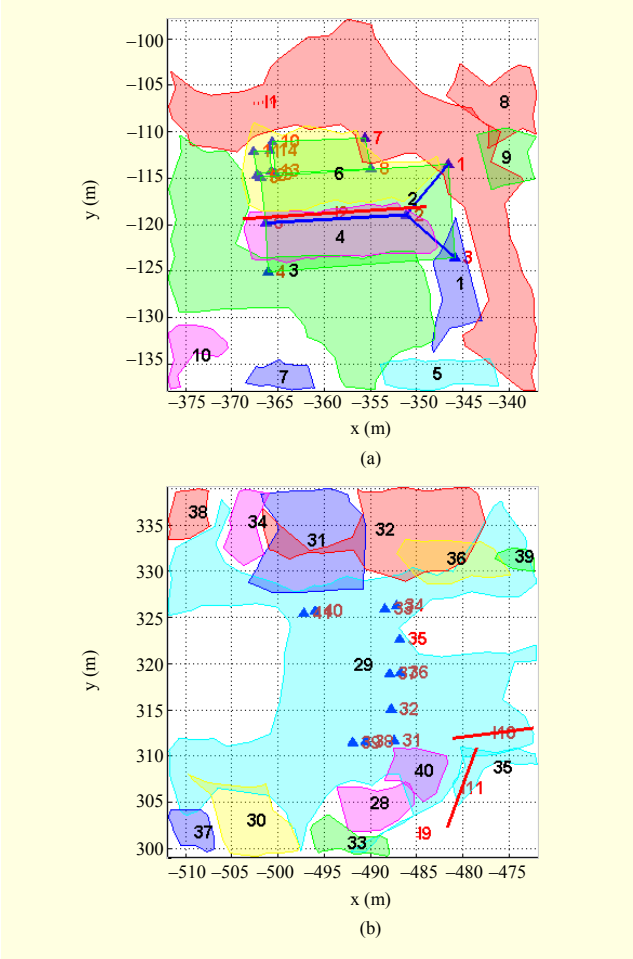

Fig. 11. (a) Patches and intersection edges extracted from LIDAR data in region A and (b) image-derived object points in region C.

EOPs of images to minimize the discrepancies between both data sets.

Before performing the data fusion processes to generate DSMs, orthoimages, or building models, we should eliminate the geometric discrepancy between the images and LIDAR data as much as possible. Hence, we attempted to readjust the EOPs of the images so that the geometry derived from the stereo-image could be more precisely registered with that from the LIDAR data. To incorporate the LIDAR data as the control information into the bundle block adjustment of the EOPs of the images, we extracted planar surface patches from the LIDAR data and derived intersection edges from the patches adjacent to each other. The nearly horizontal patches are then used as the vertical control, and the intersection edges are done as the horizontal control. As shown in Fig. 11, 10 surface patches and one intersection edge are extracted from the LIDAR data in region A. The intersection edge derived from patches 4 and 6 can be used as horizontal control by constraining the corresponding edge derived from the stereo-images, the edge linking points 2 and 6. Similarly, patch 29 in region C can be used as vertical control by constraining the corresponding image derived object points, point 31 to 44.

Table 5. EOPs at each step.

Image	EOPs	Initial given by GPS/INS	Adjusted with TP, GPS/INS	Adjusted with TP, GPS/INS, LIDAR
1	Xc1 (m)	–579.040	–579.036	–579.049
	Yc1 (m)	–84.381	–84.382	–84.372
	Zc1 (m)	1,620.500	1,620.493	1,620.515
	ω1 (°)	–2.058	–2.059	–2.039
	ϕ1 (°)	–3.316	–3.316	–3.272
	κ1 (°)	–75.602	–75.604	–75.608
2	Xc2 (m)	–214.960	–214.964	–214.982
	Yc2 (m)	23.148	23.149	23.146
	Zc2 (m)	1,617.900	1,617.933	1,617.914
	ω2 (°)	–1.280	–1.279	–1.264
	ϕ2 (°)	–2.917	–2.917	–2.858
	κ2 (°)	–75.298	–75.300	–75.301

After checking the horizontal and vertical discrepancies between the primitives extracted from each data set, we then established their correspondence. In this procedure, the proper threshold values were selected by considering the uncertainty included each data set, as presented in Table 4. From these corresponding primitives, we derived 44 vertical and 10 horizontal constraints. These constraints together with 159 pairs of the tie points and the GPS/INS data were then used for the bundle block adjustment to adjust the EOPs and the coordinates of the object points.

Table 5 shows the EOPs at each step. The first column shows the initial values provided by the GPS/INS. The second one shows the adjusted values resulted from the bundle block adjustment with the tie points and the GPS/INS data. The last one shows the adjusted values resulted from the bundle block adjustment with the tie points, the GPS/INS data, and the LIDAR derived control primitives.

Table 6. Discrepancies before and after the registration.

Discrepancies	Before registration		After registration	
	Avg.	Std.	Avg.	Std.
dX (m)	0.486	0.2695	0.005	0.0082
dY (m)	0.257	0.7174	0.003	0.0124
dZ (m)	1.437	0.3840	0.001	0.0010

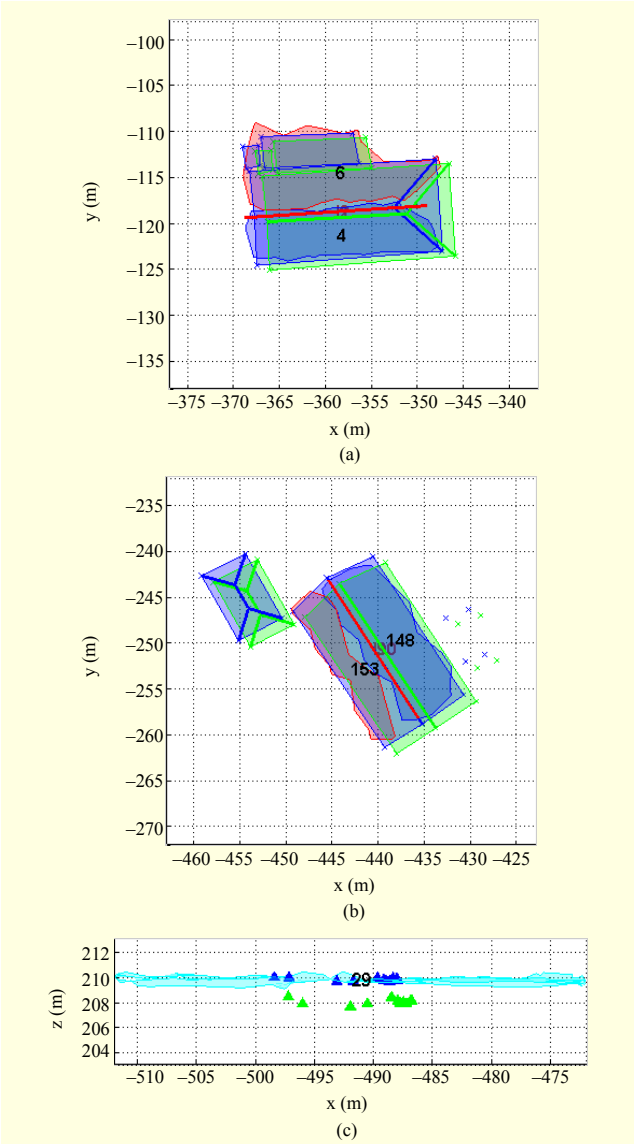

Fig. 12. Comparison of image-derived object points before and after LIDAR-based registration in regions A and L.

The EOP differences do not appear very significant, but they make significant changes on the coordinates of the object points. The average coordinate changes of the 159 object points in *X*, *Y*, and *Z* axes are about –1.430 m, 0.385 m, and 1.366 m, respectively. Figure 12 shows the image-derived geometry before and after LIDAR based registration. The green lines and points indicate the geometry before the registration, while the blue ones indicate the geometry after the registration. The central intersection edges derived from the stereo-images are exactly matched to those derived from the LIDAR data. Before the registration, the object points retain the vertical differences of 1 m to 2 m from the LIDAR patch. After registration, the points locate themselves with precision on the patch. We measured the discrepancies before and after the registration to evaluate the performance of our proposed registration method. The results are presented as Table 6. The proposed registration method could reduce the discrepancies from the range of 0.5 m through 2 m to less than 0.05 m.

IV. Conclusion

In this study, we proposed a novel method to simultaneously register images with LIDAR data using areal and linear primitives as ground control features. The main processes of the proposed method are (i) extracting registration primitives from images and LIDAR data, (ii) establishing correspondence between both primitive sets, and (iii) adjusting the exterior orientation parameters of the images.

From the comparison analysis of real data sets, we found that the images and LIDAR data retained the recognizable systematic difference although the individual data set had been carefully calibrated. The average differences were about 0.49 m, 0.26 m, 1.44 m in *X*, *Y*, and *Z* coordinates, respectively. By applying the proposed registration process to these data sets, we were able to register them precisely with the differences of less than 0.05 m.

The proposed precise registration method can be used as an intermediate process toward further information extraction processes, such as generation of accurate and dense urban DSMs, city models, and orthoimages, by combining both imagery and LIDAR data. Our future research will focus on increasing the degree of automation in extraction of registration primitives and their correspondence establishment.

References

[1] K. Choi and I. Lee, "Image Georeferencing Using AT without GCPs for a UAV-based Low-Cost Multisensor System," *Korean J. Geomatics*, vol. 27, no. 2, Apr. 2009, pp. 249-260.

[2] K. Choi et al., "Developing a UAV-Based Rapid Mapping System for Emergency Response," *Proc. SPIE*, vol. 7332, 2009, pp. 733209-733209-12.

[3] K. Choi et al, "A Project Overview for the Development of a Light and Flexible Rapid Mapping System for Emergency Response,"

Proc. 21st ISPRS Congress, 2008, pp. 915-920.

[4] A. Habib, M. Ghanma, and E.-M. Kim, "LIDAR Data for Photogrammetric Georeferencing," *Proc. FIG Working Week and GSDI-8*, 2005.

[5] S.W. Shin et al., "Algorithms for Multi-sensor and Multi-primitive Photogrammetric Triangulation," *ETRI J.*, vol. 29, no. 4, Aug. 2007, pp. 411-420.

[6] T. Schenk and C. Bea, "Fusion of LIDAR Data and Aerial Imagery for a Complete Surface Description," *Int. Archives Photogrammetry Remote Sens.,* 2002, pp. 310-317.

[7] R. Ma, *Building Model Reconstruction from LIDAR Data and Aerial Photographs,* PhD Dissertation, Ohio State University, 2004.

[8] L. Chen et al., "Building Reconstruction from LIDAR Data and Aerial Imagery," *Proc. IEEE Int. Geosci. Remote Sens. Symp.*, 2005, pp. 2846-2849.

[9] D. Lee, K. Lee, and S. Lee, "Fusion of LIDAR and Imagery for Reliable Building Extraction," *Photogrammetric Eng. Remote Sens.*, vol. 74, no. 2, Feb. 2008, pp. 215-225.

[10] D. Satale and M. Kulkami, "LIDAR in Mapping," *Map India Conf. GIS Development*, 2003. http://www.gisdevelopment.net/technology/gis/mio03129.htm (Laser accessed March 28, 2006)

[11] L. Chen, T. Teo, Y. Shao, Y. Lai, and J. Rau, "Fusion of LIDAR Data and Optical Imagery for Building Modeling," *Int. Archives Photogrammetry Remote Sens.*, vol. 35, no. B4, 2004, pp. 732-737.

[12] A. Habib and T. Schenk, "A New Approach for Matching Surfaces from Laser Scanners and Optical Sensors," *Int. Archives Photogrammetry Remote Sens.*, vol. 35, no. 3W14, 1999, pp. 55-61.

[13] P. Ronnholm et al., "Registration of Airborne Laser Scanning Point Clouds with Aerial Images through Terrestrial Image Blocks," *ISPRS J.*, vol. 37, part B1, Dec. 2008, pp. 473-479.

[14] W. Zhao, D. Nister, and S. Hsu, "Alignment of Continuous Video onto 3D Point Cloud," *Proc. CVPR,* 2004, pp. 1305-1318.

[15] C. Dold and C. Brenner, "Registration of Terrestrial Laser Scanning Data Using Planar Patches and Image Data," *IAPRS J.*, vol. 36, no. 5, Sept. 2006, pp. 78-83.

[16] K. Al-Manasir and C.S. Fraser, "Automatic Registration of Terrestrial Laser Scanner Data via Imagery," " *IAPRS J.*, vol. 36, no. 5, Sept. 2006, pp. 26-31.

[17] E. Heinrich and O. Timm, "Utilization of Ground Control Points for Image Orientation without Point Identification in Image Space," *Proc. SPIE*, 1994, pp. 206-211.

[18] J. Kilian, N. Haala, and M. Englich, "Capture and Evaluation of Airborne Laser Scanner Data," *Int. Archives Photogrammetry Remote Sens.*, 1996, pp. 383-388.

[19] T.S. Kwak et al., "Registration of Aerial Imagery and Aerial LiDAR Data Using Centroids of Plane Roof Surfaces as Control Information," *KSCE J. Civil Eng.*, vol. 10, no. 5, Sept. 2006, pp. 365-370.

[20] I. Lee, S.J. Kim, and Y. Choi, "Surface-Based Geometric Registration of Aerial Images and LIDAR Data," *Korean J. Geomatics*, vol. 5, no. 1, Dec. 2005, pp. 35-42.

[21] A. Habib et al., "Photogrammetric and LIDAR Data Registration Using Linear Features," *Photogrammetric Eng. Remote Sens.*, vol. 71, no. 6, June 2005, pp. 699-707.

[22] L. Wang and U. Neumann, "A Robust Approach for Automatic Registration of Aerial Images with Untextured Aerial LiDAR Data," *IEEE Conf. Computer Vision Pattern Recognition*, June 2009, pp. 2623-2630.

[23] L. Liu and I. Stamon, "A Systematic Approach for 2D-Image to 3D-Range Registration in Urban Environments," *Proc. Workshop Virtual Representations Modeling Large-Scale Environments,* 2007.

[24] A. Habib, M. Ghanma, and E. Mitishita, "Photogrammetric Georeferencing Using LIDAR Linear and Aerial Features," *Korean J. Geomatics*, vol. 5, no. 1, Dec. 2005, pp. 7-19.

[25] J.B. Lee and K.Y. Yu, "Co-Registrarion of Aerial Photos, ALS Data and Digital Maps Using Linear Features," *KOGSIS J.*, vol. 14, no. 4, Dec. 2006, pp. 37-44.

[26] A. Habib, Y. Lee, and M. Morgan, "Bundle Adjustment with Self-Calibration of Line Cameras Using Straight Lines," *Proc. Joint Workshop of ISPRS WG I/2, I/5 and IV/7*, 2001, unpaginated CD-ROM.

[27] I. Lee, K. Choi, and Y. Choi, "Geometric Registration of Aerial Images with LIDAR Data Using Planar Surface Patches as Control Information," *Proc. ASPRS Annual Conf.*, 2007.

[28] I. Lee, *Perceptual Organization of Surfaces*, PhD Dissertation, Ohio State University, 2002.

Kyoungah Choi received the BSc and MSc from the Department of Geoinformatics, University of Seoul, Korea, in 2006 and 2008, respectively. She is a PhD candidate at the same department. Since 2009, she has been a team leader of the Laboratory for Sensor and Modeling (LSM). Her research interests include multisensor integration, mobile mapping systems, UAV photogrammetry, real-time (or rapid) mapping, and omni-directional image processing.

Juseok Hong received the BSc and MSc from the Department of Geoinformatics, University of Seoul, Korea, in 2008 and 2010, respectively. He was a member of the Laboratory for Sensor and Modeling (LSM), from 2007 to 2010. He is now working as a research engineer at Technical Research Center, GSM Solutions Inc. His research interests include multisensor integration, mobile mapping systems, UAV photogrammetry, and the 3D stereo omni-directional camera system.

Impyeong Lee received the BSc from the Department of Electrical and Electronic Engineering, KAIST, Korea, 1991, the MSc in spacecraft technology and satellite communications from University College London, UK, 1992, and the PhD in geodetic science and surveying from Ohio State University, USA, 2002. From 1992 to 1999, he worked at Satellite Technology Research Center, KAIST and Byrd Polar Research Center, Ohio State University, 2002 and 2003. Since 2003, he has been a faculty member of Department of Geoinformatics, University of Seoul and has led the Laboratory for Sensor and Modeling (LSM). His research interests include multisensor integration, mobile mapping systems, UAV photogrammetry, real-time (or rapid) mapping, omni-directional image processing, and LIDAR simulation, processing, and forest applications.